

Response to reviewer#1

Comment: This study deals with a very interesting and important issue, i.e., parameterization of aerosol refractive index, which is essential for the estimation of aerosol direct radiative forcing. I read the manuscript and the authors' response with great interest. However, after careful evaluation, I agree with the other reviewer that this study is not suitable for publication in ACP as "it needs further analysis, reorganization, discussion and clarification to (prove) improve the confidence of the results (reviewer 1)". I will expand a bit on these issues as detailed below.

Reply: We thank the anonymous reviewer's comments. However, we can not agree with some of the reviewer's main opinions about our manuscript. Her/His comments are addressed point-by-point and our responses are listed below. More importantly, she/he evaluated our manuscript with wrong conclusion from wrong data. We have no idea how she/he obtained our first-hand field data. We would like to provide her/him the raw data for re-analysis.

Comment: Major Comments:

The parameterization scheme of the current study ($Re = (RRI2-1)/(RRI2+2) = 0.18re_{ff}$) is in principle a justification / an update of the scheme proposed by Liu and Daum (2008) ($Re = (RRI2-1)/(RRI2+2) = 0.23re_{ff}^{0.39}$) based on a new dataset measured at Taizhou in China for 7 days in June 2018. The major concern from the other reviewers is whether the new parameterization is universal and applicable in global and climate models as suggested by the authors. I am not convinced by the author's arguments because of the following reasons.

1. Is the new scheme universal and better than the one from Liu and Daum (2008)?

Reply: The new proposed parameterization scheme has been proved to be universal and applicable with more measurements data at PKU beside that at Taizhou in the revised manuscript. The results are shown in fig. R1 (figure 10 in the manuscript). We also compared the measured and calculated RRI using the corresponding data published before (Guyon et al., 2003; Hand and Kreidenweis, 2002; Hänel, 1968;

Tang, 1996; Tang and Munkelwitz, 1994). We got an R^2 of 0.91, slope of 1.00 and intercept of 0.01. Therefore, our parameterization scheme works for both our field measurement data and the previous studies. Moreover, our proposed parameterization scheme is more acceptable in physics. By definition, the RRI of mono-component particle is defined as

$$\frac{RRI^2-1}{RRI^2+2} = \frac{N_A \alpha}{3M} \rho_{\text{eff}}, \quad (1)$$

where N_A is the universal Avagadro's number, α is the mean molecular polarizability, M is the molecular weight of the material and ρ_{eff} is the mass effective density of the chemical component. When compared with equation 1, our parameterization scheme is more acceptable than that of Liu and Daum (2008). Based on above results and discussion, our parameterization scheme is universal and applicable.

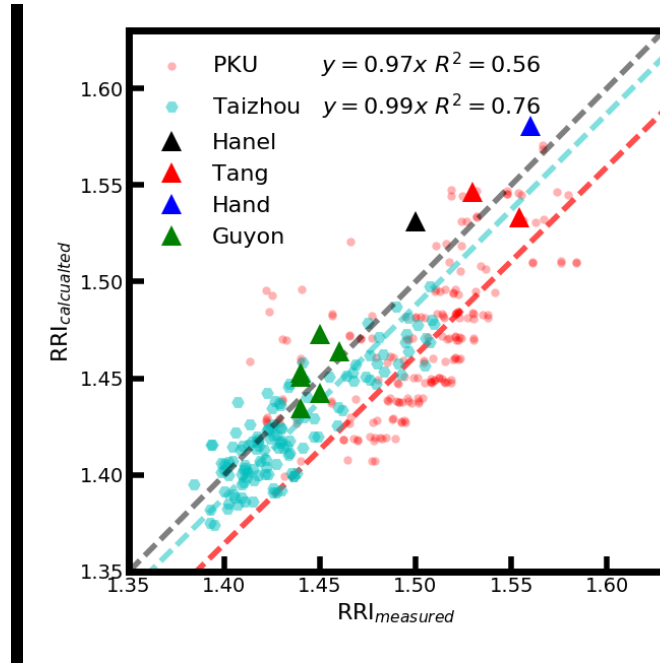


Figure R1. Comparison between the measured and calculated RRI at PKU (in red circle) and Taizhou (in cyan hexagon) station. The triangle in black , red, blue and green corresponding the data from Hänel (1968), Tang (1996), Hand and Kreidenweis (2002), and Guyon et al. (2003) respectively. The black line is the 1:1 line.

Comment: If a scheme is universal, it should not only explain one dataset, but also be applicable and compatible for other datasets. To come up with their parameterization scheme, Liu and Daum (2008) studied the relationship of refractive index to mass

density (index density relationship) for over 4000 pure materials and for aerosol particles. Note that, in Liu and Daum (2008), the summarized pure materials include organics, and investigated aerosol data cover aerosol samples from Amazon (Guyon et al., 2003), which is expected to constitute significant fraction of organics. Thus, it is not appropriate for the authors to make a statement “the influence of organic aerosols components on aerosol RRI is not considered in their work (L270-271)”.

Reply: Thanks for the comments. We agree with the reviewer that some of the description in our manuscript is not appropriately stated and we made revisions in L270-271. In Liu and Daum et al., they summarized 4000 pure materials and some aerosol data. However, the ambient aerosol particles are far from pure materials. We compared the measured and calculated RRI using their parameterizations scheme with the data before (Guyon et al., 2003; Hand and Kreidenweis, 2002; Hänel, 1968; Tang, 1996; Tang and Munkelwitz, 1994) and found our parameterization scheme behaved better than Liu and Daum’s parameterization scheme as shown in fig. R2. Furthermore, the calculated RRI using the parameterization scheme of Liu et al is biased using our field measurement data as shown in Figure 8 in our manuscript. Our parameterization scheme works well for both the data from our field measurement results and from the previous studies (Guyon et al., 2003; Hand and Kreidenweis, 2002; Tang, 1996; Tang and Munkelwitz, 1994).

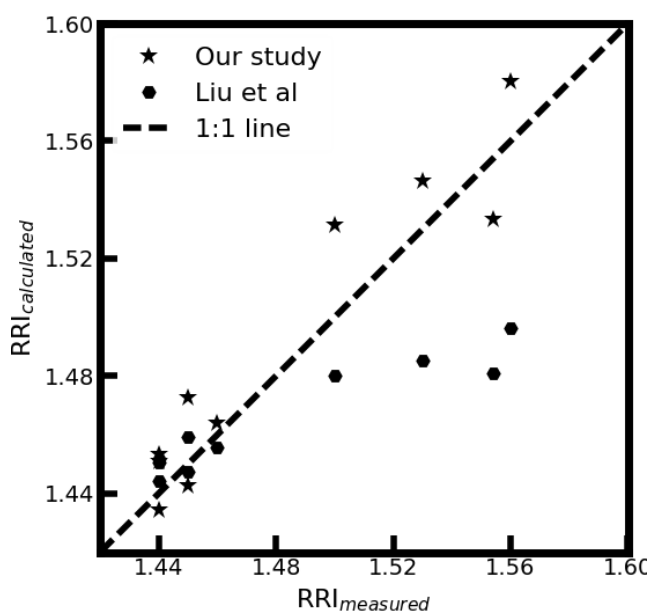


Figure R2. Comparison between the measured and calculated RRI with our parameterization scheme (star) and that of Liu's (hexagon) respectively, using the data from studies before (Guyon et al., 2003; Hand and Kreidenweis, 2002; Hänel, 1968; Tang, 1996; Tang and Munkelwitz, 1994).

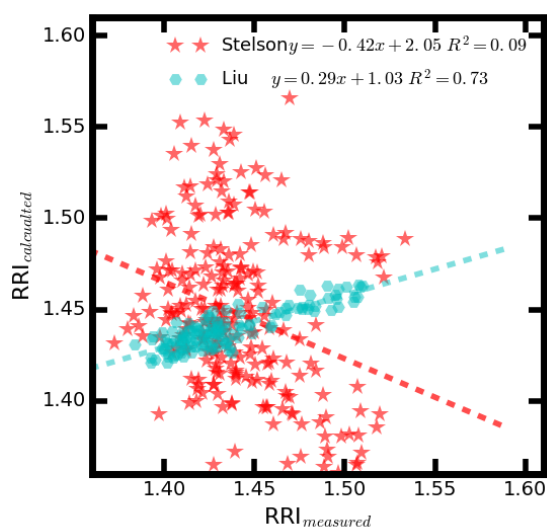


Figure 8. Comparison between the measured RRI and calculated RRI using the main aerosol chemical component with the method of Stelson (1990) (in red star) and parameterization scheme proposed by Liu and Daum (2008) (in cyan hexagon).

Comment: In Fig. C1, I compared the results of the current study with Liu and Daum (2008) by overlaying the data from the Taizhou site (small light blue dots) and from the PKU site (small pink dots) onto the original Fig. 3 of Liu and Daum (2008). Interestingly, the new datasets are not much different from the ones already summarized by Liu and Daum (2008), as they fit well into the data clouds within the same mass density range.

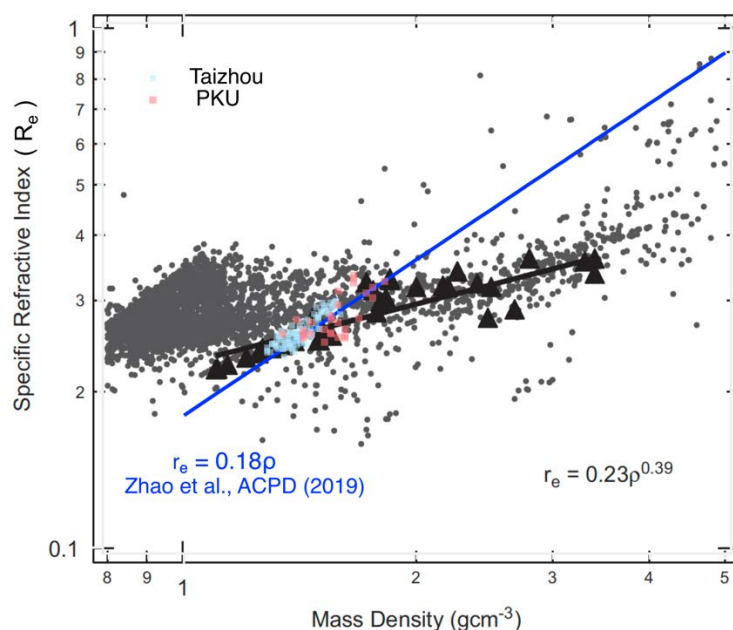


Fig. C1. Dependence of the effective refractive index ($R_e = (RRI-1)/(RRI+2)$) on the effective mass density (ρ_{eff}) for pure materials and for aerosol particles. The new data sets from the current study (small light blue dots for Taizhou and small pink dots for PKU) overlay the original Fig. 3 of Liu and Daum (2008). The data summarized by Liu Daum (2008) includes over 4000 pure materials (small grey dots, including organics, inorganics and minerals, www.knovel.com), as well as ambient aerosol and lab generated surrogate with chemical compositions representing ambient aerosols (big black triangles) (Hänel, 1968; Tang and Munkelwitz, 1994; Hand and Kreidenweis, 2002; Guyon et al. 2003).

Reply: The results which the anonymous reviewer provided in Fig.C1 are not acceptable. She/He plotted and analyzed with the wrong data. We would like to provide her/him the raw dataset to re-evaluate our manuscript. We are wondering how she/he obtained our firsthand field data which is not available to other groups.

The data from Liu and Daum comes from 4000 pure materials. However, ambient aerosol particles are far from pure materials. The chemical compositions of ambient aerosols are complicated including inorganics, organics and black carbon. Most of the mentioned pure materials in Liu and Daum (2008) rarely exist in the ambient aerosol. Thus, most of the pure materials have negligible influence on the ambient aerosol RRI. In dealing with the ambient RRI calculation, it is not proper to consider

all the 4000 pure materials, which may leading to great uncertainties. Our measured data representing the ambient aerosol properties fit into the data clouds in Liu and Daum because there were so many inappropriate data in their figure.

Comment: For the whole data population, it appears that Liu and Daum's scheme (black solid line) is still the best approach to describe the overall index-density relationship.

Reply: We do not agree with the reviewer's comments and the reasons are listed as following:

1. In the figure 8 of our manuscript, the parameterization scheme proposed by Liu and Daum failed to describe the relationship between the effective density and RRI of our measured data.

2. Liu and Daum used many data with effective density larger than 2.0 g/cm^3 . Many studies found that the ambient aerosol effective density was lower than 2.0 g/cm^3 (Hand and Kreidenweis, 2002; Lee et al., 2009; Ma et al., 2017; Qiao et al., 2018; Rissler et al., 2014; Wang et al., 2010). Only the measured results in Hänel (1968) reported that the ambient aerosol density may larger than 2.0 g/cm^3 . However, they mentioned that "It has been estimated that the systematic errors can reach the magnitude of the measuring errors" using their proposed method. These data with effective density larger than 2.0 g/cm^3 should not be used to represent the ambient aerosol properties.

3. Liu and Daum also used the data of 4000 pure materials. However, ambient aerosol particles are far from pure materials. The chemical compositions of ambient aerosols are complicated including inorganics, organics and black carbon. Most of the mentioned pure materials in Liu and Daum (2008) rarely exist in the ambient aerosol. Thus, most of the pure materials have negligible influence on the ambient aerosol RRI. In dealing with the ambient RRI calculation, it is not proper to consider all the 4000 pure materials, which may leading to great uncertainties.

Therefore, the parameterization scheme from Liu et al may not applicable for the ambient aerosol because their results are significantly influenced by the inappropriate

data.

Comment: Because the new parametrization from the current study (blue solid line) is not able to represent the general trend in the existing dataset (over 4000 pure materials marked by small grey dots), especially it failed to explain the aerosol data from early field campaign/laboratory studies (marked by big black triangles).

Reply: As mentioned above, the data from Liu and Daum comes from 4000 pure materials. However, ambient aerosol particles are far from pure materials. It is not proper to consider all the 4000 pure materials, which may leading to great uncertainties.

The reviewer concluded that our parameterization failed to explain the aerosol data from early field campaign. However, our proposed parameterization scheme works well for both our field measurement data and the early field campaign/laboratory studies as shown in fig. R1 and fig. R2. We added the comparison in the revised manuscript.

Comment: Depending on to which degree one would like the schemes to represent the variability, for the Taizhou site the predicted average RRI (~1.44) by Liu and Daum's scheme is in a reasonable agreement with the observed 28-day average RRI of 1.425, 1.435 and 1.47 for 200 nm, 300 nm and 450 nm particles, respectively, which is probably already good enough for global and climate model applications.

Reply: From fig. 8 in our manuscript, the parameterization scheme of Liu failed to fit our measured data as it biased from 1:1 line. Our parameterization scheme is better than that of Liu et al. because it works well for both our field measurement data and the early field campaign/laboratory studies as shown in fig. R1 and fig. R2.

Comment: On the other hand, when speaking of explaining the detailed temporal and spatial variability, the prediction of the new parameterization at the PKU site is quite scattered with $y = 1.0x$ and $R^2 = 0.03$ (see my Major Comments 2). For example, a prediction of RRI ~1.5 with the new parameterization scheme at the PKU site may

correspond to a variability of real/observed RRI from 1.42 to 1.58 (Fig. C2-A).

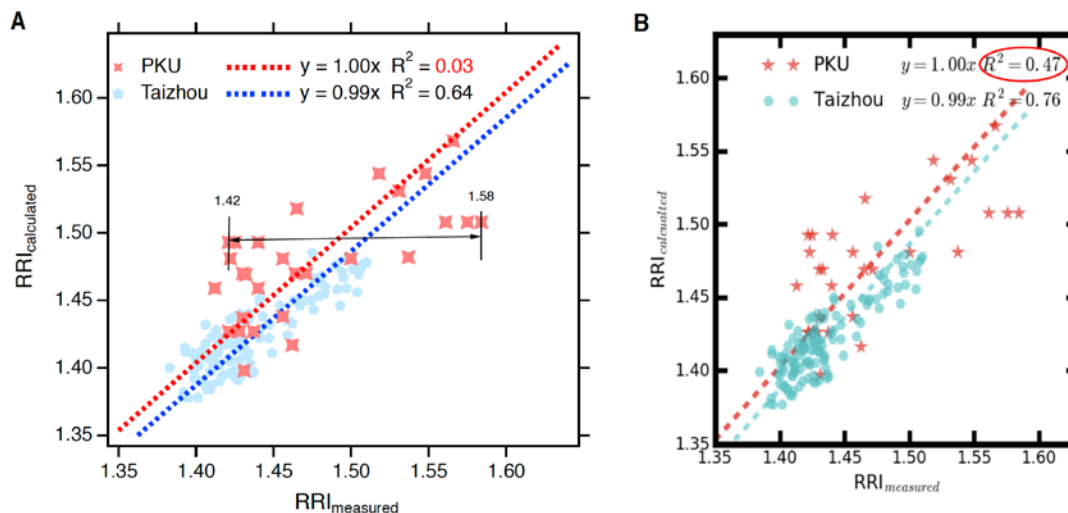


Fig. C2. Comparison of measured and predicted RRI by the parameterization scheme of Zhao et al. (ACPD). A, my re-calculation with data from Fig. 6 of Zhao et al. (ACPD). B, the original Fig. 6 of Zhao et al. (ACPD).

Reply: Again, the reviewer plotted Fig.C2 with wrong data and the results are questionable. We would like to provide the raw data for her/him to re-analysis. Also, in the revised manuscript, we added more experiment datasets at PKU site to validate our proposed parameterization scheme.

Comment: Thus, it is unlikely that the new parameterization scheme from the current study is universal and applicable to global and climate models. In my opinion, the intrinsic scattering of the index-density relationship (Fig. C1) implies that a perfect parameterization may not be even possible. If a compromise has to be made, Liu and Daum's scheme still seems to be optimal choice in terms of universality.

Reply: Based on our responses above, we do not agree with the reviewer's comment. Our parameterization scheme works well for both our own measured data and the previous published data. The parameterization scheme of Liu fails to repeat our field measurement data.

Comment: Consistence between the PKU and Taizhou sites?

When comparing the consistency of different dataset, I find that I cannot reproduce

the results of Fig. 6 in the revised manuscript (also shown here as Fig. C2-B).

While the authors provided a R^2 of 0.47 for the PKU site (Fig. C2-B), using the same fit function ($y = ax$ by forcing intercept = 0), I received a coefficient of determination (R^2) of only 0.03 for the same dataset (Fig. C2-A), not sufficient to support the authors' argument about consistence between the PKU and Taizhou sites. Apparently, the authors have selected the “good” slope (1.0) of $y = ax$ and the “better” R^2 (0.47) of $y = ax + b$ to justify the advantage of their method in Fig. 6 and relevant text. This is misleading. Such a way of selectively presenting results is a serious issue and has to be corrected.

Reply: We double checked our data and results. It is not acceptable that the reviewer evaluated our work with wrong dataset. Her/His results are questionable. We have no idea how the reviewer get our firsthand dataset. Anyway, we would like to provide her/him the raw dataset for re-analysis.

***Comment:** Other Comments:1. Abstract: The retrieved RRI is for pure scattering aerosols (or may be extended for the coating materials when calculating the effective refractive index of mixed black particles?), while the effective density is measured for all aerosols (both scattering and absorbing aerosols). Direct comparison between the two measured quantifies may induce uncertainties, and should be justified or at least clarified.*

Reply: Thanks for the comments. The following discussions would prove that the measured effective density corresponding to these of scattering aerosols. The effects of absorbing aerosols can be neglected.

Fig. R3 gave three examples of the aerosol PNSDs that had passed the CPMA and were measured by the SMPS. The mass values of the aerosol that can pass through the CPMA were set to be 12 fg, 1 fg and 1.4 fg respectively. From fig. R3, the aerosols that passed through the CPMA were mainly composed of three modes. For each mode, the aerosol number concentrations were fit by the log-normal distribution function:

$$N(H) = \frac{N_0}{\sqrt{2\pi}\log(\sigma_g)} \cdot \exp\left[-\frac{\log Dp - \log(Dp)}{2\log^2(\sigma_g)}\right] \quad (2)$$

Where σ_g is the geometric standard deviation; Dp is the geometric mean diameter and N_0 is the number concentrations for a peak mode. The geometric mean diameter is further analyzed.

We would demonstrate that the mode 1, 2 and 3 in the figure correspond to those aerosols of absorbing aerosol, scattering aerosol, and scattering aerosol with double charges respectively.

Based on the principle of CPMA, when the CPMA is selecting the aerosols at mass m_0 of single charged aerosol particles. Then theses multiple-charged (numbers of charges is n) aerosol particles with mass concentration of nm_0 can pass through the CPMA at the same time. We assume that the geometric diameter of the single charge aerosol particles is D_0 , and the effective density among different aerosol diameter doesn't have significant variations. Then the geometric diameter of the multiple charged aerosol particles is $\sqrt[3]{n}m$.

As for the DMA, when a voltage (V) is applied to the DMA, only a narrow size range of aerosol particles, with the same electrical mobility (Z_p) can pass through the DMA (Knutson and Whitby, 1975). The Z_p is expressed as:

$$Z_p = \frac{Q_{sh}}{2\pi VL} \ln\left(\frac{r_1}{r_2}\right) \quad (3)$$

where Q_{sh} is the sheath flow rate; L is the length of the DMA; r_1 is the outer radius of annular space and r_2 is the inner radius of the annular space. The transfer function refers to the probability that a particle with a certain electrical mobility can pass through the DMA. For a given V , the transfer function is triangular-shaped, with the peaking value of 100% and a half width (HW) of

$$\Delta Z_p = Z_p \frac{Q_a}{Q_{sh}} \quad (4)$$

The aerosol Z_p , which is highly related to the aerosols diameter (D_p) and the number of elementary charges on the particle (n), is defined as:

$$Z_p = \frac{neC(D_p)}{3\pi\mu D_p} \quad (5)$$

where e is the elementary charge; μ is the gas viscosity coefficient, $C(D_p)$ is the

Cunningham slip correction that is defined by:

$$C = 1 + \frac{2\tau}{D_p} \left(1.142 + 0.558e^{-\frac{0.999D_p}{2\tau}} \right) \quad (6)$$

where λ is the gas mean free path.

Therefore, the corresponding electrical diameter $Z_p(n)$ of the particles with n charges and diameters $\sqrt[3]{n}m$ can be calculated based on equation 5. The diameter (D_n) measured by the DMA can be calculated with electrical diameter $Z_p(n)$ and single charged particle by using equation 5 again. The relationship of the D_n and the aerosol diameter selected by the DMA can be determined by changing the aerosol D_p and charge numbers. The results are shown in fig. R4.

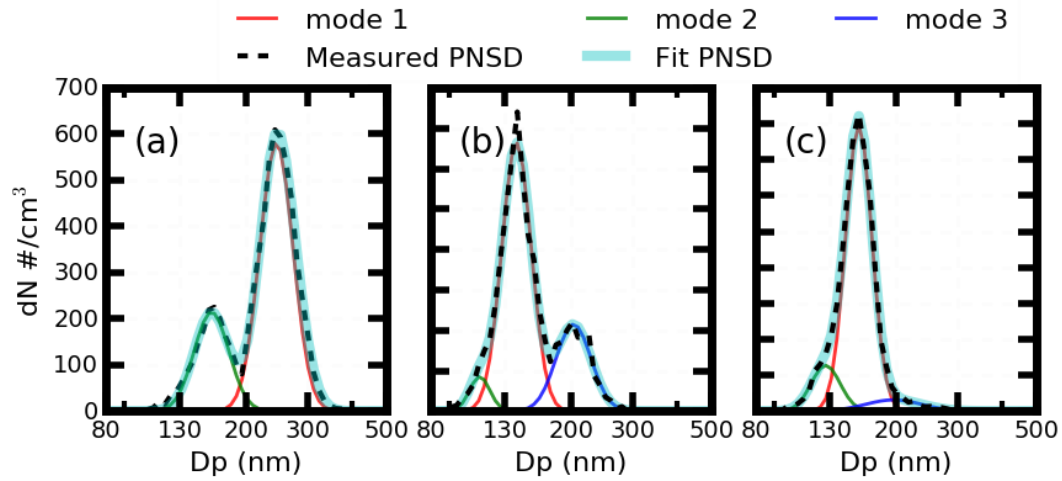


Figure R3. The measured aerosol PNSD (black dotted line), fit aerosol number PNSD (blue solid line), and fit aerosol PNSD at three different mode in different colors. Panel (a) (b) (c) corresponding to the aerosol mass concentrations of 12, 1, 1.45 fg.

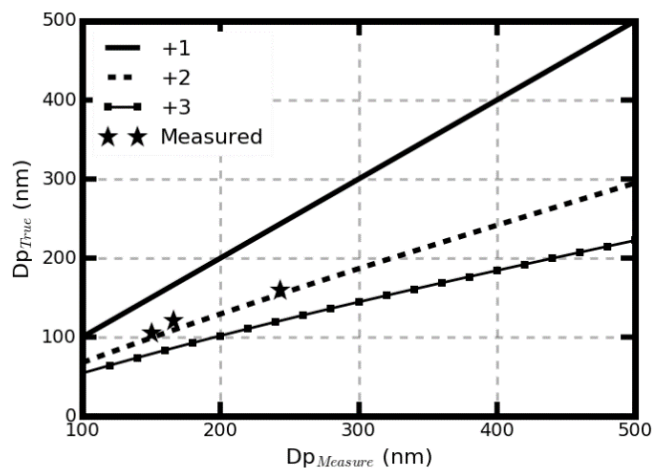


Figure R4. The relationship between the measured diameter by the DMA and the calculated true aerosol diameter of different charges in the CPMA-SMPS system.

The fit geometric diameter of mode 2 and mode 3 were also plot in fig. R4. From fig. R4, the measured relationships of the mode 2 and mode 3 agree well with that of double charged diameters. The deviations might resulted from the assumptions that the aerosol effective density doesn't change among different diameters. Therefore, we conclude that the mode 3 corresponds to the double-charged aerosols and should not be used to analyze the effective density.

However, the mode 1 and mode 2 corresponding to the effective densities around 1.0 g/cm^3 and 1.5 g/cm^3 respectively. Previous studies had shown that the ambient BC aerosol is chain like in the morphology and have smaller effective density values. At the same time, the fit aerosol number concentrations of mode one is only between 1/5 to 1/3 of the mode two. Based on the size-selected aerosol properties, there were only mean 25% percent of the ambient aerosols that contains BC (another paper in preparation). Therefore, the mode 1 corresponds to the BC-contained aerosols and mode 2 corresponds mainly to scattering aerosols.

In our study, the effective density correspond to the geometric diameters of mode 2 was used. Thus, both the measured aerosol effective density and RRI correspond to these scattering aerosols. We added the above discussion in the revised manuscript.

Comment: 2. Abstract and section 3.2: I suggest to remove “rather than the main chemical components” from “We find that the ambient aerosol RRI is highly related with the aerosol effective density (ρ_{eff}) rather than the main chemical components”, or change ‘related’ to ‘correlated’. This is because both refractive index and effective density are determined by main chemical components of aerosol particles. Even for the proposed application in global or climate model (calculation of RRI from ρ_{eff}), one would still need the simulated chemical compositions to calculate ρ_{eff} (see my Other Comments 3).

Reply: Thanks for the comments. We have revised the manuscript.

Comment: Along this line, section 3.2 should be substantially revised by including more detailed and thorough evidences and discussions. See my concerns below. The major argument/results presented in section 3.2 to support the conclusion “the ambient aerosol RRI is highly related with the aerosol effective density (ρ_{eff}) rather than the main chemical components” are Fig. 4, Fig. 5 and Fig. S6 (in the revised manuscript). However, RRI and chemical compositions in these comparisons were not taken from the same aerosol group. The RRI were taken from aerosol of a certain size (i.e., 300 nm) while the chemical compositions were taken from PM_{2.5} either for direct comparison (Fig. 4 and Fig. S6) or for calculating the RRI (Fig. 5) (The water-soluble ions were from PM_{2.5}; whether ECOC measurements were from PM_{2.5} or PM₁₀ are not clear in the text of section 2.1). In this case, even the same parameter may differ from each other. For example, one can clearly see multiple modes in the comparison of main aerosol components and RRI in Fig. S6.

Such comparison can be misleading because there is a danger that the readers might get an impression that the commonly used mixing rules in calculating refractive index wouldn't work for ambient aerosols, e.g., volume linear mixing rule, Maxwell-Garnet and Bruggemann mixing rule, partial molar refraction mixing rule, Lorentz-Lorenz mixing rule etc. (those requires information of chemical compositions in a mixed system). A direct consequence has already been shown in Fig. 5, where the authors delivered a message that Stelson's approach (Stelson, 1990) of calculating refractive

index with partial molar refraction mixing rule did not work for the Taizhou case. This is unfair because the mismatch of different aerosol population in this comparison may to some (large) extent lead to the very scattered data points of the Stelson's approach in Fig. 5.

Reply: Thanks for the comments. The ECOC measurements were from PM_{2.5}. We have changed the manuscript.

We would first demonstrate that the measured RRI at a given diameter of 250 nm is in consistent with that of the bulk aerosol optical properties derived RRI. The aerosol-effective RRI was retrieved by applying the Mie scattering theory to the aerosol particle number size distribution (PNSD), aerosol bulk scattering coefficient and aerosol absorbing coefficient data (Cai et al., 2011). Results in fig. R3 show that the measured and calculated RRI shows good consistence.

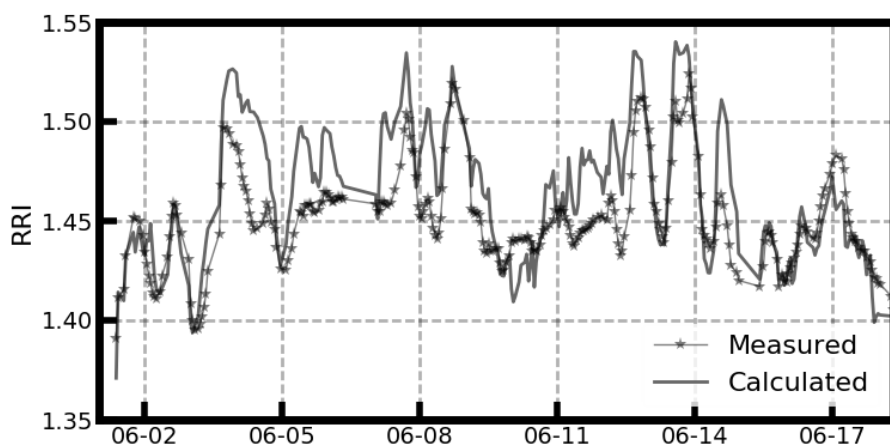


Figure. R3. Comparison between the measured RRI at 250 nm and the calculated RRI using the aerosol bulk aerosol optical properties.

Therefore, the size-resolved aerosol RRI can be used to some extent represent the bulk aerosol optical properties. The measured RRI at 250 nm and calculated aerosol RRI using the bulk aerosol main chemical composition should to some extent correlated with each other. However, as shown in fig. 5 in the manuscript, the measured RRI at 250 nm and calculated RRI using the method Stelson (1990) has R^2 of 0.07. Therefore, the ambient aerosol RRI calculated from bulk aerosol main inorganic component may lead to great uncertainties.

The commonly used mixing rules in calculating refractive index may not work for ambient aerosols. The main reason of the discrepancy are due to ignoring influence of organic. The manuscript was revised correspondingly.

Comments: 3. The authors' response about "how to use the parameterization in numerical models, i.e., what is the input and required parameters, may be required" is not adequate. Modelers understand "the effective density is the only parameter as input", but the real question is how to determine the effective density in the model, which hasn't been answered. I guess that one would still need to calculate reff from densities of individual simulated chemical composition. This procedure however, may be hampered by the lack of density information of organic carbons and mixing state of black carbon, etc.

Reply: Thanks for the comment. The motivation of our research is to bridge the gap between the ambient aerosol RRI and ambient aerosol effective density. How to determine the effective density in the model is out of the scope of our research. In fact, there are many methods available to estimate the ambient aerosol effective density (Hu et al., 2012; Karg, 2000; Qiao et al., 2018; Schmid et al., 2007; Zhang et al., 2016). The RRI can be calculated conveniently with available effective density using our parameterization scheme.

Comments:4. Concerning Reviewer 2's comment "Zhao et al. (2018b) seems to be still under discussion. The readers cannot trust the method only from the explanation in this manuscript.", the authors may want to refer to the work of Zhang et al. (JGR, 2018), where the method of combining DMA and SP2 to retrieve the real part of the refractive index of pure scattering aerosol particles has been proposed and published.

Reply: Thanks for the comment. The work of Zhao et al. (2018b) has been published as Zhao et al. (2019). The details of combining DMA and SP2 to retrieve the real part of the refractive index can be found in that.

Comment: 5. L50: "main aerosol" is duplicated.

Reply: Thanks for the comments. We have revised the manuscript.

Comment: 6. L198-199: could it be that statistics of RRI at 200 and 300 nm is better than at 450 nm? Because the scattering signal of SP2 may become saturated for a large fraction of particles at 450 nm, and reduce the sample size. How were the double charged particles treated?

Reply: Thanks for the comments. We checked the scattering signals and the scattering signal of SP2 is not saturated for these particles at 450 nm. The reason of RRI get more dispersed at 450 nm might be related the complicated aging processing and sources of these large particles compared with those at 200 nm and 300 nm. The method of treating the double charged particles are detailed in Zhao et al. (2019).

Comment: 7. L147-151: “SSA is defined as the ratio of ssca to sext, which reflects concentration of the absorbing aerosol (Tao et al., 2014) to some extent. The g expresses the distribution of the scattering light intensity in different directions (Zhao et al., 2018a). The sext, SSA and g are the most important three factors that influence the aerosol radiative properties in radiative calculation (Kuang et al., 2015).” L169-170: “... the difference between f_n^- and $f_n(f_n^- - f_n)$ is the downward radiative irradiance flux for aerosol-free conditions (Kuang et al., 2016).”

It does not seem to be appropriate to cite these references here, because such statements are rather classical textbook knowledge.

Reply: Thanks for the comment. We have revised the manuscript.

Comment: 8. L192: change “The RRI and reff vary...” to “The RRI varies”.

Reply: Thanks for the comment. We have revised the manuscript.

Comment: 9. L201-202: change “at about 15:00 in the morning” to “at about 15:00 in the afternoon” and change “at around 9:00 in the afternoon” to “at around 9:00 in the morning”.

Reply: Thanks for the comment. We have revised the manuscript.

Comment: 10. L214-215: "...Thus, the effective tend to increase with the increment of aerosol diameter." sounds like a broken sentence.

Reply: Thanks for the comment. We have deleted the corresponding content in the manuscript.

Comment: 11. L254: "one day" instead of "one days".

Reply: Thanks for the comment. We have revised the manuscript.

Comment: 12. Fig. 5: The caption is confusing and needs to be revised. "Comparison between the measured RRI and calculated RRI using the main aerosol chemical component from Stelson (1990) (in red star)..." Do the authors mean using the same aerosol chemical species those are needed for applying the Stelson's method, but the concentrations of the chemical components are still the measured ones from this study? If yes, please revise the caption. This is related to reviewer's comment about "Why do the authors compare a result with other at different time series and measurement site?"

Reply: Thanks for the comments. We have revised the manuscript.

Cai, Y., Montague, D.C., Deshler, T. (2011) Comparison of measured and calculated scattering from surface aerosols with an average, a size-dependent, and a time-dependent refractive index. *Journal of Geophysical Research* 116.

Guyon, P., Boucher, O., Graham, B., Beck, J., Mayol-Bracero, O.L., Roberts, G.C., Maenhaut, W., Artaxo, P., Andreae, M.O. (2003) Refractive index of aerosol particles over the Amazon tropical forest during LBA-EUSTACH 1999. *Journal of Aerosol Science* 34, 883-907.

Hand, J.L., Kreidenweis, S.M. (2002) A New Method for Retrieving Particle Refractive Index and Effective Density from Aerosol Size Distribution Data. *Aerosol Science And Technology* 36, 1012-1026.

Hänel, G. (1968) REAL PART OF MEAN COMPLEX REFRACTIVE INDEX AND

MEAN DENSITY OF SAMPLES OF ATMOSPHERIC AEROSOL PARTICLES.
Tellus 20, 371-&.

Hu, M., Peng, J., Sun, K., Yue, D., Guo, S., Wiedensohler, A., Wu, Z. (2012) Estimation of size-resolved ambient particle density based on the measurement of aerosol number, mass, and chemical size distributions in the winter in Beijing. Environ Sci Technol 46, 9941-9947.

Karg, E. (2000) The density of ambient particles from combined DMA and APS data. Journal of Aerosol Science 31, 759-760.

Knutson, E.O., Whitby, K.T. (1975) Aerosol classification by electric mobility: apparatus, theory, and applications. Journal of Aerosol Science 6, 443-451.

Lee, S.Y., Widiyastuti, W., Tajima, N., Iskandar, F., Okuyama, K. (2009) Measurement of the Effective Density of Both Spherical Aggregated and Ordered Porous Aerosol Particles Using Mobility- and Mass-Analyzers. Aerosol Science And Technology 43, 136-144.

Liu, Y., Daum, P.H. (2008) Relationship of refractive index to mass density and self-consistency of mixing rules for multicomponent mixtures like ambient aerosols. Journal of Aerosol Science 39, 974-986.

Ma, Y., Li, S., Zheng, J., Khalizov, A., Wang, X., Wang, Z., Zhou, Y. (2017) Size-resolved measurements of mixing state and cloud-nucleating ability of aerosols in Nanjing, China. Journal of Geophysical Research: Atmospheres 122, 9430-9450.

Qiao, K., Wu, Z., Pei, X., Liu, Q., Shang, D., Zheng, J., Du, Z., Zhu, W., Wu, Y., Lou, S., Guo, S., Chan, C.K., Pathak, R.K., Hallquist, M., Hu, M. (2018) Size-resolved effective density of submicron particles during summertime in the rural atmosphere of Beijing, China. Journal of Environmental Sciences.

Rissler, J., Nordin, E.Z., Eriksson, A.C., Nilsson, P.T., Frosch, M., Sporre, M.K., Wierzbicka, A., Svenningsson, B., Londahl, J., Messing, M.E., Sjogren, S., Hemmingsen, J.G., Loft, S., Pagels, J.H., Swietlicki, E. (2014) Effective density and mixing state of aerosol particles in a near-traffic urban environment. Environ Sci Technol 48, 6300-6308.

Schmid, O., Karg, E., Hagen, D.E., Whitefield, P.D., Ferron, G.A. (2007) On the

effective density of non-spherical particles as derived from combined measurements of aerodynamic and mobility equivalent size. *Journal of Aerosol Science* 38, 431-443.

Stelson, A.W. (1990) Urban aerosol refractive index prediction by partial molar refraction approach. *Environ.sci.technol* 24:11, 1676-1679.

Tang, I.N. (1996) Chemical and size effects of hygroscopic aerosols on light scattering coefficients. *Journal of Geophysical Research: Atmospheres* 101, 19245-19250.

Tang, I.N., Munkelwitz, H.R. (1994) WATER ACTIVITIES, DENSITIES, AND REFRACTIVE-INDEXES OF AQUEOUS SULFATES AND SODIUM-NITRATE DROPLETS OF ATMOSPHERIC IMPORTANCE. *Journal Of Geophysical Research-Atmospheres* 99, 18801-18808.

Wang, X., Zhang, L., Moran, M.D. (2010) Uncertainty assessment of current size-resolved parameterizations for below-cloud particle scavenging by rain. *Atmospheric Chemistry and Physics* 10, 5685-5705.

Zhang, G., Bi, X., Qiu, N., Han, B., Lin, Q., Peng, L., Chen, D., Wang, X., Peng, P., apos, an, Sheng, G., Zhou, Z. (2016) The real part of the refractive indices and effective densities for chemically segregated ambient aerosols in Guangzhou measured by a single-particle aerosol mass spectrometer. *Atmospheric Chemistry and Physics* 16, 2631-2640.

Zhao, G., Zhao, W., Zhao, C. (2019) Method to measure the size-resolved real part of aerosol refractive index using differential mobility analyzer in tandem with single-particle soot photometer. *Atmospheric Measurement Techniques* 12, 3541-3550.

A new parameterization scheme of the real part of the ambient aerosols refractive index

Gang Zhao¹, Tianyi Tan², Weilun Zhao¹, Song Guo², Ping Tian³, Chunsheng Zhao^{1*}

¹ Department of Atmospheric and Oceanic Sciences, School of Physics, Peking University, Beijing, China

² State Key Joint Laboratory of Environmental Simulation and Pollution Control, College of Environmental Sciences and Engineering, Peking University, Beijing 100871, China

³ Beijing Key Laboratory of Cloud, Precipitation and Atmospheric Water Resources, Beijing 100089, China

***Correspondence to: Chunsheng Zhao (zcs@pku.edu.cn)**

Abstract

The refractive index of ambient aerosols, which directly determines the aerosol optical properties, is widely used in atmospheric models and remote sensing. Traditionally, the real part of the refractive index (RRI) is mainly parameterized by the measurement of ambient aerosol main inorganic components. In this paper, the characteristics of the ambient aerosol RRI are studied based on the field measurement in the East China. Results show that the ambient aerosol RRI varies significantly between 1.36 and 1.56. The direct aerosol radiative forcing is estimated to vary by 40% corresponding to the variation of the measured aerosol RRI. We find that the ambient aerosol RRI is highly correlated with the aerosol effective density (ρ_{eff}) rather than the main chemical components. However, parameterization schemes of the ambient aerosol RRI by ρ_{eff} are not available due to the lack of corresponding simultaneous field measurements. For the first time, the size-resolved ambient aerosol

21 RRI and ρ_{eff} are measured simultaneously by our designed measurement system. A new
22 parameterization scheme of the ambient aerosols RRI using ρ_{eff} is proposed. The measured and
23 parameterized RRI agree well with the correlation coefficient of 0.75 and slope of 0.99. Knowledge of
24 the ambient aerosol RRI would improve our understanding of the ambient aerosol radiative effects.

25 **1 Introduction**

26 Atmospheric aerosols can significantly influence the regional air quality and climate system by
27 scattering and absorbing the solar radiation (Seinfeld et al., 1998). However, estimation of the aerosol
28 radiative effects remains large uncertainties due to the high temporal and spatial variations in aerosol
29 microphysical properties (Levoni et al., 1997). The complex refractive index (RI), which directly
30 determines the aerosol scattering and absorbing abilities (Bohren and Huffman, 2007), is one of the
31 most important microphysical parameters of aerosol optics and radiation. RI is widely employed in
32 atmospheric models and remote sensing (Zhao et al., 2017). When estimating the direct aerosol
33 radiative forcing (DARF), many studies showed that great uncertainties may arise due to small
34 uncertainties in the real part of the RI (RRI). It was found that a small perturbation in RRI (0.003) can
35 lead to an uncertainty of 1% in DARF for non-absorbing particles (Zarzana et al., 2014). An increment
36 of 12% in the DARF occurred when the RRI increased from 1.4 to 1.5 (Moise et al., 2015) over the
37 wavelength range between 0.2 μm and 5 μm . Therefore, it is necessary to measure or parameterize the
38 ambient aerosol RRI with high accuracy.

39 Traditionally, the RRI is derived from measurements of aerosol main inorganic chemical
40 compositions (Han et al., 2009). For the ambient aerosol with multiple components, linear volume
41 average of known aerosol chemical composition is widely used to estimate the aerosol effective
42 RRI_{eff} (Hand and Kreidenweis, 2002; Liu and Daum, 2008; Hänel, 1968; Wex et al., 2002) with :

$$43 \quad RRI_{eff} = \sum_i (f_i \cdot RRI_i) \quad (1)$$

44 Where f_i and RRI_i are the volume fraction and real part of refractive index of known composition
45 i . However, the influences of organic component on the aerosol RRI were not considered when
46 estimating the RRI using the traditional method. The organic component contributes more than 20%

47 of the total aerosol component in China (Hu et al., 2012;Liu et al., 2014). At the same time, RRI of the
48 organic aerosol changes significantly between 1.36 and 1.66 (Moise et al., 2015). Ignoring the organic
49 component may lead to significant biases when estimating the ambient aerosol RRI. The comparison
50 between the estimated RRI using ~~main-aerosol~~ main aerosol composition and measured aerosol RRI
51 using other method was not available due to the lack of measurement of ambient aerosol RRI.

52 Information of RRI may be helpful for the knowledge of ambient aerosol chemical information.
53 Many studies find that ambient aerosols of different size have different properties such as shape (Peng
54 et al., 2016), chemical composition (Hu et al., 2012) and density (Qiao et al., 2018). Up until now,
55 there is limit information about the size-resolved RRI (\widetilde{RRI}) of ambient particles. Characteristics of the
56 ambient aerosol \widetilde{RRI} were not well studied yet.

57 The RRI of mono-component particle is defined as (Liu and Daum, 2008):

$$58 \quad \frac{RRI^2 - 1}{RRI^2 + 2} = \frac{N_A \alpha}{3M} \rho_{eff} \quad (2)$$

59 where N_A is the universal Avagadro's number, α is the mean molecular polarizability, M is the
60 molecular weight of the material and ρ_{eff} is the mass effective density of the chemical component.
61 The RRI should be highly related to ρ_{eff} . However, there was no study that investigated the
62 relationship between the RRI and ρ_{eff} of ambient aerosol in China.

63 The ρ_{eff} of ambient aerosols is one of the crucial parameters in aerosol thermo-dynamical and
64 optical models. It can be used to infer the ambient particle aging process (Peng et al., 2016). Based on
65 equation 2, the aerosol ρ_{eff} is directly related to the aerosol RRI. Few studies measure the ambient
66 aerosol RRI and ρ_{eff} simultaneously. So far, parameterizations of the RRI by ρ_{eff} using the
67 simultaneous measurements are not available. Real-time measurements of the ρ_{eff} and aerosol RRI
68 concurrently can help to better understand the relationship between the aerosol RRI and ρ_{eff} .

69 In this study, the aerosol \widetilde{RRI} and size resolved ρ_{eff} ($\widetilde{\rho_{eff}}$) are measured simultaneously during
70 a field measurement conducted in Taizhou in the East China. The ambient aerosol \widetilde{RRI} is measured
71 by our designed system, which combines a differential mobility analyzer (DMA) and a single particle
72 soot photometer (SP2) (Zhao et al., 2019). The $\widetilde{\rho_{eff}}$ is measured by using a centrifugal particle mass
73 analyzer (CMPA) and a scanning mobility particle sizer (SMPS). The characteristic of the \widetilde{RRI} and
74 $\widetilde{\rho_{eff}}$ are analyzed in this study. It is the first time that the \widetilde{RRI} and $\widetilde{\rho_{eff}}$ of the ambient aerosol are

75 measured simultaneously. A parameterization scheme of the RRI by the ρ_{eff} using the simultaneous
76 measurement is proposed. Based on the measured variability of the measured RRI, we estimated the
77 corresponding variation of the aerosol direct aerosol radiative forcing, which to some extent give
78 valuable knowledge for the influence of aerosol RRI variations on aerosol radiative effects.

79 The structure of this study is as follows: the descriptions of the instrument setup is given in section
80 2.1, 2.2 and 2.3. The methodology of evaluating the aerosol optical properties and radiative effects
81 corresponding to the variations of the measured RRI are shown in section 2.4 and 2.5 respectively.
82 Section 3.1 describes the characteristics of the measured the $\widetilde{\text{RRI}}$ and $\widetilde{\rho_{\text{eff}}}$. Section 3.3 proposes the
83 parameterization of the aerosol RRI. The corresponding variations in aerosol optical properties and
84 radiative effects corresponding to the variations of the measured RRI are both discussed in section 3.4.

85 **2 Data and Methods**

86 **2.1 Description of the measurement campaign**

87 The measurement was conducted in a suburban site Taizhou (119°57'E, 32°35'N), as shown in
88 fig. 1(a), which lies in the south end of the Jianghuai Plain in the central Eastern China. It is located
89 on the north east of the megacity Nanjing with a distance of 118 km. Another megacity Shanghai is
90 200 km away from Taizhou in the southeastern direction. The industrial area between Nanjing and
91 Shanghai has experienced severe pollutions in the past twenty years. The average Moderate Resolution
92 Imaging Spectroradiometer (MODIS) aerosol optical depth data at 550nm over the year 2017, as
93 shown in fig. 1(b), also reflects that the measurement site is more polluted than the surrounding areas.

94 During the field campaign, all of the instruments were placed in a container, in which the temperature
95 was well controlled within 24 ± 2 °C. The sample air was collected from a PM₁₀ impactor (Mesa Labs,
96 Model SSI2.5) mounted on the top of the container and then passed through a Nafion dryer tube to
97 ensure that the relative humidity of the sample particles was controlled below 30%.

98 Along with the measurement of the $\widetilde{\text{RRI}}$ and $\widetilde{\rho_{\text{eff}}}$, the aerosol scattering coefficients (σ_{sca}) at three
99 different wavelengths (450, 525 and 635 nm) were measured by an nephelometer (Aurora 3000,
100 Ecotech, Australia) (Müller et al., 2011) at a resolution of 5 minutes. The scattering truncation and
101 non-Lambertian error was corrected using the same method as that of Ma et al. (2011). The aerosol

water-soluble ions (NH_4^+ , SO_4^{2-} , NO_3^- , Cl^-) of $\text{PM}_{2.5}$ were measured by an In situ Gas and Aerosol Compositions Monitor (TH-GAC3000, China). The mass concentration of elementary carbon and organic carbon (OC) of $\text{PM}_{2.5}$ were measured using a thermal optical transmittance aerosol carbon analyzer (ECOC, Focused Photonics Inc.). The concentrations of Organic matters (OM) are achieved through multiplying OC concentration by 1.4 (Hu et al., 2012). The time resolution of the aerosol composition measurement was one hour.

2.2 Measuring the $\widetilde{\text{RRI}}$

A coupling DMA-SP2 system was employed to measure the aerosol $\widetilde{\text{RRI}}$ from 24th, May to 18th, June in 2018. This system is introduced elsewhere by (Zhao et al., 2019) and a brief description is presented here. As schematically shown in fig. S42, the monodispersed aerosols selected by a DMA (Model 3081, TSI, USA) are drawn into a SP2 to measure the corresponding scattering properties. The SP2 is capable of distinguishing the pure scattering aerosols from the black carbon (BC) containing aerosols by measuring the incandescence signals at 1064 nm. For the pure scattering aerosol, the scattering strength (S) measured by SP2 is expressed as:

$$S = C \cdot I_0 \cdot (\sigma_{45^\circ} + \sigma_{135^\circ}) \quad (3),$$

where C is a constant that is determined by the instrument response character; I_0 is the instrument's laser intensity; σ_{45° and σ_{135° is the scattering function of the sampled aerosol at 45° and 135° , respectively;. From Mie scattering theory, aerosol size and RRI directly determine the scattering function at a given direction. Inversely, the aerosol RRI can be retrieved when the aerosol size and scattering strength are determined. This system can measure the ambient aerosol $\widetilde{\text{RRI}}$ with uncertainty less than 0.02 (Zhao et al., 2019).

Before the measurement, this system is calibrated with ammonia sulfate ($\text{RRI}=1.52$). ~~The relationships between the diameter and the measured scattering peak height are shown in fig. S2.~~ After calibration, ammonium chloride is used to validate the method of deriving the RRI at different aerosol diameters. The RRI value of ammonium chloride is 1.642 (Lide, 2006) and the measured RRI of ammonium chloride is in the range between 1.624 and 1.656 in our study. Therefore, this measurement system can measure the ambient aerosol RRI with high accuracy.

2.3 Measuring the $\widetilde{\rho_{\text{eff}}}$

The ρ_{eff} is measured by a Centrifugal Particle Mass Analyzer (CPMA, version 1.53, Cambustion Ltd, UK) in tandem with a Scanning Mobility Particle Sizer (SMPS) system from 12th, June to 18th, June in 2018. The ρ_{eff} is defined as

$$\rho_{\text{eff}} = \frac{m_p}{\frac{\pi}{6} \times d_m^3} \quad (4),$$

Where m_p is the particle mass and d_m is the aerosol mobility diameter selected by DMA.

The controlling of the CPMA-SMPS system is achieved by self-established Labview software. The CPMA is set to scan twelve different aerosol mass at 1.0, 1.4, 2.0, 2.9, 4.2, 5.9, 8.5, 12.1, 17.2, 24.6, 35.0 and 50.0 fg every five minutes respectively. The SMPS scan the aerosol diameters between 60nm and 500nm every 5 minute, which results in a period of one hour for measuring the effective density of different mass.

At the beginning of the field measurement, the CPMA-SMPS system is calibrated using the PSL particles with different mass. The corresponding measured effective densities of PSL particles are 1.04 and 1.07 g/cm³, which agree well with the PSL material density of 1.05 g/cm³.

Fig. 3 gave three examples of the aerosol PNSDs that passed the CPMA and were measured by the SMPS. The mass values of the aerosol that can pass through the CPMA were set to be 12, 1 and 1.4 fg respectively. From fig. 3, these aerosols that pass through the CPMA were mainly composed of three modes. For each mode, the aerosol number concentrations were fit by log-normal distribution function:

$$N(H) = \frac{N_0}{\sqrt{2\pi} \log(\sigma_g)} \cdot \exp \left[-\frac{\log Dp - \log(Dp)}{2 \log^2(\sigma_g)} \right], \quad (5)$$

where σ_g is the geometric standard deviation; Dp is the geometric mean diameter and N_0 is the number concentrations for a peak mode. The geometric mean diameter is further analyzed.

We would demonstrate the mode 1, 2 and 3 in fig. 3 correspond to those aerosols of absorbing aerosol, scattering aerosol, and scattering aerosol with double charges respectively.

Based on the principle of CPMA, when the CPMA is selecting the aerosols at mass m_0 of single charged aerosol particles. Theses multiple-charged (numbers of charges is n) aerosol particles with

mass concentration of nm_0 can pass through the CPMA at the same time. We assumed that the geometric diameter of the single charge aerosol particles was D_0 , and the effective density among different aerosol diameter didn't have significant variations. Thus, the geometric diameter of the multiple charged aerosol particles is $\sqrt[3]{n}m$.

As for the DMA, when a voltage (V) is applied to the DMA, only a narrow size range of aerosol particles, with the same electrical mobility (Z_p) can pass through the DMA (Knutson and Whitby, 1975). The Z_p is expressed as:

$$Z_p = \frac{Q_{sh}}{2\pi VL} \ln\left(\frac{r_1}{r_2}\right) \quad (6)$$

where Q_{sh} is the sheath flow rate; L is the length of the DMA; r_1 is the outer radius of annular space and r_2 is the inner radius of the annular space. The aerosol Z_p , which is highly related to the aerosols diameter (D_p) and the number of elementary charges on the particle (n), is defined as:

$$Z_p = \frac{neC(D_p)}{3\pi\mu D_p} \quad (7)$$

where e is the elementary charge; μ is the gas viscosity coefficient, $C(D_p)$ is the Cunningham slip correction that is defined by:

$$C = 1 + \frac{2\tau}{D_p} \left(1.142 + 0.558e^{-\frac{0.999D_p}{2\tau}}\right) \quad (8)$$

where τ is the gas mean free path.

Therefore, the electrical diameter $Z_p(n)$ of the particles with n charges and diameters $\sqrt[3]{n}m$ can be calculated based on equation 5. Thus, the corresponding diameter (D_n) measured by the DMA can be calculated with electrical diameter $Z_p(n)$ and single charged particle by using equation 5 again. The relationship of the D_n and the aerosol diameter selected by the DMA can be determined by changing the aerosol D_p and charge numbers. The results were shown in fig. 4.

The fit geometric diameters of mode 2 and mode 3 were also shown in fig. 4. From fig. 4, the measured diameter relationships of the mode 2 and mode 3 agree well with the calculated one between the single charged and double charged diameters. The little deviation might result from the

assumptions that the aerosol effective density doesn't change among different diameters. We concluded that the mode 3 corresponds to the double-charged aerosols. Mode 3 is not used in our study.

Mode 1 and mode 2 corresponding to the effective densities around 1.0 g/cm^3 and 1.5 g/cm^3 . Previous studies have shown that the ambient BC aerosol was chain like in the morphology and had smaller effective density values (Peng et al., 2016). At the same time, the fit aerosol number concentrations of mode one is only between 1/5 to 1/3 of the mode two. Based on the size-selected aerosol properties measured by the SP2, there were only mean 25% percent of the ambient aerosols that contains BC. Therefore, the mode 1 and mode 2 corresponded to the BC-contained aerosols and scattering aerosols respectively.

The effective density used in our study correspond to the geometric diameters of mode 2. Thus, both the measured aerosol effective density and RRI correspond to these scattering aerosols

2.4 Calculate aerosol optical properties using different RRI

The aerosol optical properties are highly related to the RRI. From Mie scattering theory, the variation in aerosol RRI may result in significant variations in the aerosol optical properties, such as aerosol extinction coefficient (σ_{ext}), the σ_{sca} , the single scattering albedo (SSA), and the asymmetry factor (g) (Bohren and Huffman, 2007). ~~SSA is defined as the ratio of σ_{sca} to σ_{ext} , which reflects concentration of the absorbing aerosol (Tao et al., 2014) to some extent. The g expresses the distribution of the scattering light intensity in different directions (Zhao et al., 2018).~~ The σ_{ext} , SSA and g are the most important three factors that influence the aerosol radiative properties in radiative calculation (Kuang et al., 2015; Zhao et al., 2018).

In this study, the sensitivity studies of the aerosol optical properties to the aerosol RRI are carried out by employing the Mie scattering theory. The input variables of Mie scattering model includes the aerosol PNSD and BC mixing state and aerosol complex refractive index. The Mie model can calculate the σ_{ext} , σ_{sca} , SSA and g . The mixing state of the ambient BC comes from the measurements of the DMA-SP2 system. All of the aerosols are divided into pure scattering aerosols and BC-containing aerosols. The BC-containing aerosols are assumed to be core-shell mixed. As for the RI of BC,

205 1.8+0.54i is used (Kuang et al., 2015). With this, the aerosol σ_{ext} , σ_{sca} , SSA and g at different RRI
206 values can be calculated.

207 2.5 Estimating the aerosol DARF

208 In this study, the DARF under different aerosol RRI conditions is estimated by the Santa Barbara
209 DISORT (discrete ordinates radiative transfer) Atmospheric Radiative Transfer (SBDART) model
210 (Ricchiazzi et al., 1998). Under the cloud-free conditions, DARF at the TOA is calculated as the
211 difference between radiative flux under aerosol-free conditions and aerosol present conditions:

212
$$\text{DARF} = (f_{\text{a}} \downarrow - f_{\text{a}} \uparrow) - (f_{\text{ff}} \downarrow - f_{\text{ff}} \uparrow) \quad (5),$$

213 where $f_{\text{a}} \downarrow$ and $f_{\text{a}} \uparrow$ are the downward and upward radiative irradiance with aerosol present
214 conditions respectively; the difference between $f_{\text{a}} \downarrow$ and $f_{\text{a}} \uparrow$ ($f_{\text{a}} \downarrow - f_{\text{a}} \uparrow$) is the downward radiative
215 irradiance flux with aerosol present conditions; $f_{\text{ff}} \downarrow$ and $f_{\text{ff}} \uparrow$ correspond to the downward and
216 upward radiative irradiance values under aerosol free conditions respectively; the difference between
217 $f_{\text{ff}} \downarrow$ and $f_{\text{ff}} \uparrow$ ($f_{\text{ff}} \downarrow - f_{\text{ff}} \uparrow$) is the downward radiative irradiance flux for aerosol free conditions
218 (Kuang et al., 2016). The instant DARF value is calculated over the wavelength range between 0.25
219 μm and 4 μm .

220 Input data for the model are shown below. The vertical profiles of temperature, pressure and water
221 vapor, which adopt the radiosonde observations at Taizhou site. The measured mean results
222 corresponding the field measurement period are used. Vertical distributions of aerosol σ_{ext} , SSA and
223 g with a resolution of 50 m, are resulted from the calculation using the Mie Model and parameterized
224 aerosol vertical distributions. Methods for parameterization and calculation of the aerosol optical
225 profiles can be found in ~~Sect. S3 or in~~ Zhao et al. (2018). The surface albedo adopt the mean results of
226 MODIS V005 Climate Modeling Grid (CMG) Albedo Product (MCD43C3) at the area of Taizhou
227 from May, 2017 to April, 2018. The other default values are used in the simulation (Ricchiazzi et al.,
228 1998).

229 3 Results and Discussions

230 3.1 The Measurements Results

231 The overview of the measurement is shown in fig. 25. During the measurement, the σ_{sca} is
232 relatively low with a mean value of $167 \pm 74 \text{ Mm}^{-1}$. There were one major pollution episodes occurred

based on the σ_{sca} time series as shown in fig. 25(a). This pollution happens on 13th, June and doesn't last long. The corresponding σ_{sca} reaches 540 Mm⁻¹. A moderate polluted condition between 14th, June and 15th, June is observed. The aerosol PNSD changes substantially with the pollution conditions as shown in fig. 25(b). The geometric median aerosol diameter changes between 30 nm and 105 nm. The median diameter tends to be lower when the surrounding is cleaner. Despite the median diameter reaches 105 nm on 16th, June, the surrounding is relative clean due to the low aerosol number concentration. The $\widetilde{\text{RRI}}$ ~~and $\widetilde{\rho_{\text{eff}}}$ varies~~ from 1.34 to 1.54 and the $\widetilde{\rho_{\text{eff}}}$ ranges between 1.21 to 1.80 g/cm³ as shown in fig. 25(c) and (d). From fig. 52, the measured RRI shows the same variation pattern with the ρ_{eff} . Both the $\widetilde{\text{RRI}}$ and $\widetilde{\rho_{\text{eff}}}$ increase with the diameter, which may indicate that the aerosol chemical composition varies among different aerosol particle size.

As for the $\widetilde{\text{RRI}}$, the corresponding mean RRI values for aerosol diameter at 200nm, 300nm and 450nm are 1.425 ± 0.031 , 1.435 ± 0.041 , 1.47 ± 0.059 . When comparing the probability distribution of the RRI for different diameter in fig. 36, the RRI is more dispersed when the particle size increases, implicating that the aerosol compositions become complicated when the aerosol get aged. Fig. 3-6(a), (c) and (e) give diurnal variation of the $\widetilde{\text{RRI}}$ values at different particle sizes of 200 nm, 300 nm and 450 nm. The RRI shows diurnal cycles for different diameters. They reach the peak at about 15:00 in the ~~morning~~ afternoon and fall to the valley at around 9:00 in the ~~afternoon~~ morning.

The range of the measured RRI (1.34~1.56) is a little wider than the literature values. The past measurement of the ambient aerosol RRI values varies between 1.4 and 1.6 (Dubovik, 2002; Guyon et al., 2003; Zhang et al., 2016) over different measurement site. This is the first time that such high variations in ambient aerosol RRI were observed at one site.

The $\widetilde{\rho_{\text{eff}}}$ shows almost the same diurnal variations as the $\widetilde{\text{RRI}}$ as shown fig. 55S1. The diurnal variations of the $\widetilde{\rho_{\text{eff}}}$ is more dispersed because the time period of measuring the $\widetilde{\rho_{\text{eff}}}$ is shorter (7 days) comparing with the time of $\widetilde{\text{RRI}}$ (28 days). It is evident that the ρ_{eff} increased with particle size. The difference of ρ_{eff} among different particle size should be resulted from different contributions of chemical compositions, especially the OM. Based on the previous measurement of the size-resolved chemical compositions using a micro orifice uniform deposit impactors (MOUDI), the mass fraction of OM get decreased with the increment of aerosol diameter (Hu et al., 2012). At the

same time, the effective density of OM is lower than the other main inorganic compositions. ~~Thus, the effective tend to increase with the increment of aerosol diameter.~~

3.2 Aerosol Chemical Composition versus the RRI

From equation (1) and (2), the aerosol RRI can be determined by aerosol chemical composition (Liu and Daum, 2008). Many studies calculate the RRI using the measurement results of the relative contributions of aerosol chemical composition (Yue et al., 1994; Hänel, 1968; Guyon et al., 2003; Stelson, 1990; Wex et al., 2002). However, there is no comparison between the RRI calculated from chemical composition and real-time measurement until now. In this study, the relationship between the measured RRI and the mass fraction of each ion components is investigated.

As illustrated in fig. 47, the RRI tend to increase with the OM mass fraction ratio, which implies that the OM may play an important role in aerosol scattering properties. This is in agreement with the Aldhaif et al. (2018), where the aerosol OM contributes a lot to the ambient aerosol mass concentrations. The RRI have implicit relationship with the mass fraction of the σ_{sca} at 525 nm, SO_4^{2-} , Cl^- , and NO_3^- . The mass ratio of NH_4^+ seems to be negatively correlated with the RRI. At the same time, the measured RRI values have no clear relationship with the absolute mass concentrations of the main aerosol chemical components, as shown in fig. S6S2.

The RRI is also calculated by applying the method proposed by Stelson (1990), in which the bulk chemical composition is used. The comparison between the calculated RRI and the measured RRI is shown in fig. 58. It can be noticed that the calculated RRI and the measured RRI doesn't agree well. There are several reasons that may cause the discrepancies. The first reason might be that the aerosol chemical information used in the method is the average mass of whole aerosol population. The aerosol chemical composition may vary significantly among different size. Secondly, the OM of the ambient aerosols is very complicated and the influence of the OM on the aerosol RRI has not been studied well. Therefore, more research is necessary when parameterizing the ambient aerosol RRI with the measured aerosol chemical composition.

We would demonstrate that the measured RRI at a given diameter of 250 nm is in consistent with that of the bulk aerosol optical properties derived RRI. The aerosol-effective RRI of bulk aerosol was retrieved by applying the Mie scattering theory to the aerosol particle number size distribution (PNSD).

aerosol bulk scattering coefficient and aerosol absorbing coefficient data (Cai et al., 2011). Fig. 9 shows the time series of measured and retrieved aerosol RRI. Results in fig. 9 show that the measured and calculated RRI shows good consistence with $R^2 = 0.59$. Therefore, the size-resolved aerosol RRI can be used to represent the bulk aerosol optical properties. The measured RRI at 250 nm and calculated aerosol RRI using the bulk aerosol main chemical composition should to some extent correlated with each other. However, as shown in fig. 8, the measured RRI at 250 nm and calculated RRI using the method Stelson (1990) has R^2 of 0.07. Therefore, the ambient aerosol RRI calculated from bulk aerosol main inorganic component may lead to great uncertainties.

3.3 Parameterizing the RRI using ρ_{eff}

As shown in fig. 25, there is good consistence between the variation of the measured \widetilde{RRI} and $\widetilde{\rho}_{eff}$. When defining the specific refractive index Re with $Re = \frac{RRI^2 - 1}{RRI^2 + 2}$, we found that the Re is highly correlated with ρ_{eff} by a R^2 equaling 0.75 and slope 0.99 (fig. 510). The linear relationships between the Re and ρ_{eff} is:

$$\frac{RRI^2 - 1}{RRI^2 + 2} = 0.18\rho_{eff} \quad (96).$$

The RRI can be calculated based on equation 6:

$$RRI = \sqrt{\frac{1 + 0.36\rho_{eff}}{1 - 0.18\rho_{eff}}} \quad (107).$$

Based on equation 97 and fig. 6-10 the aerosol RRI can be parameterized by the ρ_{eff} with high accuracy and the uncertainties of the calculated RRI using equation 7-10 can be constrained within 0.025. The aerosol ρ_{eff} is easier to be measured, and equation 7-10 might be used as a good probe of parameterizing the RRI.

To demonstrate the universality of this parameterization scheme, we conducted another measurement in the campus of Peking University (PKU) (N39°59', E116°18'), in North China Plain, where the aerosol effective density and real part of the refractive index are measured concurrently at from 16th to 20st, December in 2018. ~~The measurement last only one days because some instruments were borrowed from other institute.~~ The RRI were also calculated using the parameterization scheme equation 7. The slope and correlation coefficient at PKU site are ~~0.971-0~~ and ~~0.47-56~~ respectively. The

calculated and measured RRI show good consistence. Therefore, this scheme is applicable for different seasons at both Center China and North China Plain. We also compared the measured RRI and calculated RRI using the measured ρ_{eff} that have been previously published (Hänel, 1968; Tang and Munkelwitz, 1994; Tang, 1996; Hand and Kreidenweis, 2002; Guyon et al., 2003). The measured and calculated RRI show good consistence with R^2 of 0.91 and slope of 1.0. Therefore, our parameterization scheme is universal and applicable.

This parameterization scheme is easy to use because the effective density is the only parameter used as input. We have demonstrated that the traditional method of calculating the RRI using aerosol main chemical components can have significant bias because the effects of organic aerosol is not considered. The RRI can be easy to calculate based on our parameterization scheme, as the effective density of ambient aerosol is rather easier to measure.

In the previous, Liu and Daum (2008) summarized some of the measured RRI and the ρ_{eff} , and parameterized the RRI as

$$\frac{\text{RRI}^2 - 1}{\text{RRI}^2 + 2} = 0.23\rho^{0.39} \quad (8).$$

The feasibility of this scheme is tested here and the results are shown in fig. 58. The measured and parameterized RRI using the method of Liu and Daum (2008) deviated from 1:1 line. The relationship of the effective density and RRI were mainly from 4000 pure materials and few ambient aerosol data. However, the ambient aerosol were far from pure materials. At the same time, most of the pure materials have negligible contribution to the total aerosol. Therefore, the parameterization scheme from Liu and Daum (2008) can't well describe the relationships of the effective density and RRI of ambient aerosol. The effective density and RRI in their work were estimated using the aerosol chemical components but not the field measurement. At the same time, the influence of organic aerosols components on aerosol RRI is not considered in their work.

3.4 Influence of RRI Variation on Aerosol Optical Properties and Radiative Properties

The measured RRI varies between 1.34 and 1.56 during the field campaign. The corresponding aerosol optical properties are estimated. When estimating the aerosol optical properties with different aerosol RRI, the measured mean aerosol PNSD and mixing states are used. Fig. 711 gives the variation

of the aerosol σ_{sca} , SSA and g . From fig. 711, the σ_{sca} varies from 162 Mm^{-1} to 308 Mm^{-1} . The SSA varies between 0.843 and 0.895, which matches the variations of the dry aerosol SSA for different aerosol size distributions in the North China Plain (NCP) (Tao et al., 2014). As for the aerosol g , it decreases from 0.667 to 0.602 with the increment of the aerosol RRI. The ambient g values in the NCP are found within 0.55 and 0.66 (Zhao et al., 2018). Thus, the variations of the RRI have significant influence on the g . The aerosol optical properties change significantly with the variation of the ambient aerosol RRI.

The instant DARF values under different RRI are also estimated and the results are illustrated in fig. 711(b). When the aerosol RRI increases from 1.4 to 1.5, the DARF varies from -6.17 to -8.35, corresponding to 15% variation in DARF. This values are in accordance with the work of Moise et al. (2015), who estimate that an increment of 12% in the DARF occurs when the RRI varies from 1.4 to 1.5. The DARF can change from -4.9 w/m^2 to -10.14 w/m^2 when the aerosol RRI increase from 1.34 to 1.56, which corresponding to 40% variation in DARF. Great uncertainties may arise when estimating the aerosol radiative forcing when using a constant RRI. The RRI should be different under different aerosol conditions. The real time measured RRI should be used rather than a constant RRI when estimating the ambient aerosol optical and radiative properties. However, the real-time measurement of ambient aerosol RRI is not available for most of the conditions. Our proposed parameterizations scheme is a perfect substitute. The only parameter required is aerosol effective density and it is much easier to measure.

4 Conclusions

The ambient aerosol RRI is a key parameter in determining the aerosol optical properties and knowledge of it can help constrain the uncertainties in aerosol radiative forcing. In this study, the ambient aerosol $\widetilde{\text{RRI}}$ were measured at Taizhou, in the Jianghuai Plain of China by using a DMA in tandem with a SP2 from 24th, May to 18th, June in 2018.

Results show that the ambient aerosol RRI varies over a wide range between 1.34 and 1.56. The RRI increases slowly with the increment of the aerosol diameter. The mean aerosol RRI values are 1.425 ± 0.031 , 1.435 ± 0.041 , 1.47 ± 0.059 for aerosol diameter at 200 nm, 300 nm and 450 nm

respectively. Probability distributions of the RRI show that the RRI is more dispersed with the increment of aerosol diameter, which reflect the complexing aging processing of the ambient aerosol. The aerosol optical properties change significantly and the DARF is estimated to vary by 40% corresponding to the variation of the measured ambient aerosol RRI. The real-time measured RRI should be used rather than a constant RRI when estimating the ambient aerosol optical and radiative properties.

Traditionally, the ambient aerosol RRI is mainly calculated by using the corresponding measured main chemical inorganic compositions of aerosols. We find that the ambient aerosol RRI is highly correlated with the ρ_{eff} rather than the main chemical compositions of aerosols. There is discrepancy between the measured and parameterized RRI using the traditional method. This might be resulted from two reasons. The first one is that the aerosol chemical information used for calculation is the total aerosol loading. The aerosol chemical compositions may change significantly among different size. Another one is that the influence of OM of ambient aerosols is not considered. The RRI of OM varies significantly for different compositions (Moise et al., 2015).

Despite that the RRI is correlated with the ρ_{eff} , parameterization scheme of the ambient aerosol RRI using ρ_{eff} is not available due to the lack of simultaneously measurement. For the first time, the $\widetilde{\text{RRI}}$ and $\widetilde{\rho_{\text{eff}}}$ were measured simultaneously using our designed system. The $\widetilde{\rho_{\text{eff}}}$ is measured during the field campaign by employing a CMPA and a SMPS from 12th, June to 18th, June in 2018.

A new parameterization scheme of the ambient aerosol RRI using the ρ_{eff} is proposed based on the field measurement results. The measured and parameterized RRI agree well with the correlation coefficient of 0.75 and slope of 0.99. This parameterization scheme is validated at another measurement site at different season. This simple scheme is reliable and ready to be used in the calculation of aerosol optical and radiative properties. The corresponding measurement results can also be further used in climate model.

Competing interests. The authors declare that they have no conflict of interest.

395 **Data availability.** The data used in this study is available when requesting the authors.

396 **Author contributions.** GZ, CZ, WZ and SG designed and conducted the experiments; PT, TY and
397 GZ discussed the results.

398 **Acknowledgments.** This work is supported by the National Natural Science Foundation of China
399 (41590872) and National Key R&D Program of China (2016YFC020000:Task 5).

400 **References**

- 401 Aldhaif, A. M., Stahl, C., Braun, R. A., Moghaddam, M. A., Shingler, T., Crosbie, E., Sawamura, P.,
402 Dadashazar, H., Ziemba, L., Jimenez, J. L., Campuzano-Jost, P., and Sorooshian, A.: Characterization
403 of the Real Part of Dry Aerosol Refractive Index Over North America From the Surface to 12 km,
404 Journal of Geophysical Research: Atmospheres, 10.1029/2018jd028504, 2018.
- 405 Bohren, C. F., and Huffman, D. R.: Absorption and Scattering by a Sphere, in: Absorption and
406 Scattering of Light by Small Particles, Wiley-VCH Verlag GmbH, 82-129, 2007.
- 407 Cai, Y., Montague, D. C., and Deshler, T.: Comparison of measured and calculated scattering from
408 surface aerosols with an average, a size-dependent, and a time-dependent refractive index, Journal of
409 Geophysical Research, 116, 10.1029/2010jd014607, 2011.
- 410 Dubovik, O.: Variability of absorption and optical properties of key aerosol types observed in
411 worldwide locations, J.atmos.sci, 59, 590-608, 2002.
- 412 Guyon, P., Boucher, O., Graham, B., Beck, J., Mayol-Bracero, O. L., Roberts, G. C., Maenhaut, W.,
413 Artaxo, P., and Andreae, M. O.: Refractive index of aerosol particles over the Amazon tropical forest
414 during LBA-EUSTACH 1999, Journal of Aerosol Science, 34, 883-907, 10.1016/s0021-
415 8502(03)00052-1, 2003.
- 416 Han, Y., Lü, D., Rao, R., and Wang, Y.: Determination of the complex refractive indices of aerosol
417 from aerodynamic particle size spectrometer and integrating nephelometer measurements, Applied
418 Optics, 48, 4108-4117, 10.1364/AO.48.004108, 2009.
- 419 Hand, J. L., and Kreidenweis, S. M.: A New Method for Retrieving Particle Refractive Index and
420 Effective Density from Aerosol Size Distribution Data, Aerosol Sci. Technol., 36, 1012-1026,
421 10.1080/02786820290092276, 2002.

422 Hänel, G.: REAL PART OF MEAN COMPLEX REFRACTIVE INDEX AND MEAN DENSITY OF
 423 SAMPLES OF ATMOSPHERIC AEROSOL PARTICLES, *Tellus*, 20, 371-&
 424 10.3402/tellusa.v20i3.10016, 1968.

425 Hu, M., Peng, J., Sun, K., Yue, D., Guo, S., Wiedensohler, A., and Wu, Z.: Estimation of size-resolved
 426 ambient particle density based on the measurement of aerosol number, mass, and chemical size
 427 distributions in the winter in Beijing, *Environ Sci Technol*, 46, 9941-9947, 10.1021/es204073t, 2012.

428 Knutson, E. O., and Whitby, K. T.: Aerosol classification by electric mobility: apparatus, theory, and
 429 applications, *Journal of Aerosol Science*, 6, 443-451, [https://doi.org/10.1016/0021-8502\(75\)90060-9](https://doi.org/10.1016/0021-8502(75)90060-9),
 430 1975.

431 Kuang, Y., Zhao, C. S., Tao, J. C., and Ma, N.: Diurnal variations of aerosol optical properties in the
 432 North China Plain and their influences on the estimates of direct aerosol radiative effect, *Atmos. Chem.*
 433 *Phys.*, 15, 5761-5772, 10.5194/acp-15-5761-2015, 2015.

434 Kuang, Y., Zhao, C. S., Tao, J. C., Bian, Y. X., and Ma, N.: Impact of aerosol hygroscopic growth on
 435 the direct aerosol radiative effect in summer on North China Plain, *Atmospheric Environment*, 147,
 436 224-233, 2016.

437 Levoni, C., Cervino, M., Guzzi, R., and Torricella, F.: Atmospheric aerosol optical properties: a
 438 database of radiative characteristics for different components and classes, *Appl Opt*, 36, 8031-8041,
 439 1997.

440 Lide, D. R.: Handbook of Chemistry and Physics, 86th Edition Edited(National Institute of Standards
 441 and Technology), *Journal of the American Chemical Society*, 128, 5585-5585, 10.1021/ja059868l,
 442 2006.

443 Liu, H. J., Zhao, C. S., Nekat, B., Ma, N., Wiedensohler, A., van Pinxteren, D., Spindler, G., Müller,
 444 K., and Herrmann, H.: Aerosol hygroscopicity derived from size-segregated chemical composition and
 445 its parameterization in the North China Plain, *Atmospheric Chemistry and Physics*, 14, 2525-2539,
 446 10.5194/acp-14-2525-2014, 2014.

447 Liu, Y., and Daum, P. H.: Relationship of refractive index to mass density and self-consistency of
 448 mixing rules for multicomponent mixtures like ambient aerosols, *Journal of Aerosol Science*, 39, 974-
 449 986, 10.1016/j.jaerosci.2008.06.006, 2008.

450 Ma, N., Zhao, C. S., Nowak, A., Müller, T., Pfeifer, S., Cheng, Y. F., Deng, Z. Z., Liu, P. F., Xu, W.
451 Y., Ran, L., Yan, P., Göbel, T., Hallbauer, E., Mildenerger, K., Henning, S., Yu, J., Chen, L. L., Zhou,
452 X. J., Stratmann, F., and Wiedensohler, A.: Aerosol optical properties in the North China Plain during
453 HaChi campaign: an in-situ optical closure study, *Atmos. Chem. Phys.*, 11, 5959-5973, 10.5194/acp-
454 11-5959-2011, 2011.

455 Moise, T., Flores, J. M., and Rudich, Y.: Optical properties of secondary organic aerosols and their
456 changes by chemical processes, *Chemical Reviews*, 115, 4400-4439, 2015.

457 Müller, T., Laborde, M., Kassell, G., and Wiedensohler, A.: Design and performance of a three-
458 wavelength LED-based total scatter and backscatter integrating nephelometer, *Atmos. Meas. Tech.*, 4,
459 1291-1303, 10.5194/amt-4-1291-2011, 2011.

460 Peng, J., Hu, M., Guo, S., Du, Z., Zheng, J., Shang, D., Levy Zamora, M., Zeng, L., Shao, M., Wu, Y.-
461 S., Zheng, J., Wang, Y., Glen, C. R., Collins, D. R., Molina, M. J., and Zhang, R.: Markedly enhanced
462 absorption and direct radiative forcing of black carbon under polluted urban environments,
463 *Proceedings of the National Academy of Sciences*, 113, 4266-4271, 10.1073/pnas.1602310113, 2016.

464 Qiao, K., Wu, Z., Pei, X., Liu, Q., Shang, D., Zheng, J., Du, Z., Zhu, W., Wu, Y., Lou, S., Guo, S.,
465 Chan, C. K., Pathak, R. K., Hallquist, M., and Hu, M.: Size-resolved effective density of submicron
466 particles during summertime in the rural atmosphere of Beijing, China, *Journal of Environmental*
467 *Sciences*, 10.1016/j.jes.2018.01.012, 2018.

468 Ricchiazzi, P., Yang, S., Gautier, C., and Sowle, D.: SBDART: A Research and Teaching Software
469 Tool for Plane-Parallel Radiative Transfer in the Earth's Atmosphere, *Bulletin of the American*
470 *Meteorological Society*, 79, 2101-2114, 10.1175/1520-0477(1998)079<2101:sarats>2.0.co;2, 1998.

471 Seinfeld, J. H., Pandis, S. N., and Noone, K.: Atmospheric Chemistry and Physics: From Air Pollution
472 to Climate Change, *Environment Science & Policy for Sustainable Development*, 40, 26-26, 1998.

473 Stelson, A. W.: Urban aerosol refractive index prediction by partial molar refraction approach,
474 *Environ.sci.technol*, 24:11, 1676-1679, 1990.

475 Tang, I. N., and Munkelwitz, H. R.: WATER ACTIVITIES, DENSITIES, AND REFRACTIVE-
476 INDEXES OF AQUEOUS SULFATES AND SODIUM-NITRATE DROPLETS OF

477 ATMOSPHERIC IMPORTANCE, J Geophys Res-Atmos, 99, 18801-18808, 10.1029/94jd01345,
 478 1994.

479 Tang, I. N.: Chemical and size effects of hygroscopic aerosols on light scattering coefficients, Journal
 480 of Geophysical Research: Atmospheres, 101, 19245-19250, 10.1029/96jd03003, 1996.

481 Tao, J. C., Zhao, C. S., Ma, N., and Liu, P. F.: The impact of aerosol hygroscopic growth on the single-
 482 scattering albedo and its application on the NO₂ photolysis rate coefficient, Atmos. Chem. Phys., 14,
 483 12055-12067, 10.5194/acp-14-12055-2014, 2014.

484 Wex, H., Neusüß, C., Wendisch, M., Stratmann, F., Koziar, C., Keil, A., Wiedensohler, A., and Ebert,
 485 M.: Particle scattering, backscattering, and absorption coefficients: An in situ closure and sensitivity
 486 study, Journal of Geophysical Research: Atmospheres, 107, LAC 4-1-LAC 4-18,
 487 10.1029/2000jd000234, 2002.

488 Yue, G. K., Poole, L. R., Wang, P. H., and Chiou, E. W.: STRATOSPHERIC AEROSOL ACIDITY,
 489 DENSITY, AND REFRACTIVE-INDEX DEDUCED FROM SAGE-II AND NMC
 490 TEMPERATURE DATA, J Geophys Res-Atmos, 99, 3727-3738, 10.1029/93jd02989, 1994.

491 Zarzana, K. J., Cappa, C. D., and Tolbert, M. A.: Sensitivity of Aerosol Refractive Index Retrievals
 492 Using Optical Spectroscopy, Aerosol Sci. Technol., 48, 1133-1144, 10.1080/02786826.2014.963498,
 493 2014.

494 Zhang, G., Bi, X., Qiu, N., Han, B., Lin, Q., Peng, L., Chen, D., Wang, X., Peng, P., apos, an, Sheng,
 495 G., and Zhou, Z.: The real part of the refractive indices and effective densities for chemically
 496 segregated ambient aerosols in Guangzhou measured by a single-particle aerosol mass spectrometer,
 497 Atmospheric Chemistry and Physics, 16, 2631-2640, 10.5194/acp-16-2631-2016, 2016.

498 Zhao, G., Zhao, C., Kuang, Y., Tao, J., Tan, W., Bian, Y., Li, J., and Li, C.: Impact of aerosol
 499 hygroscopic growth on retrieving aerosol extinction coefficient profiles from elastic-backscatter lidar
 500 signals, Atmospheric Chemistry and Physics, 17, 12133-12143, 10.5194/acp-17-12133-2017, 2017.

501 Zhao, G., Zhao, C., Kuang, Y., Bian, Y., Tao, J., Shen, C., and Yu, Y.: Calculating the aerosol
 502 asymmetry factor based on measurements from the humidified nephelometer system, Atmospheric
 503 Chemistry and Physics, 18, 9049-9060, 10.5194/acp-18-9049-2018, 2018.

504 Zhao, G., Zhao, W., and Zhao, C.: Method to measure the size-resolved real part of aerosol refractive
505 index using differential mobility analyzer in tandem with single-particle soot photometer, *Atmospheric*
506 *Measurement Techniques*, 12, 3541-3550, 10.5194/amt-12-3541-2019, 2019.

507

508

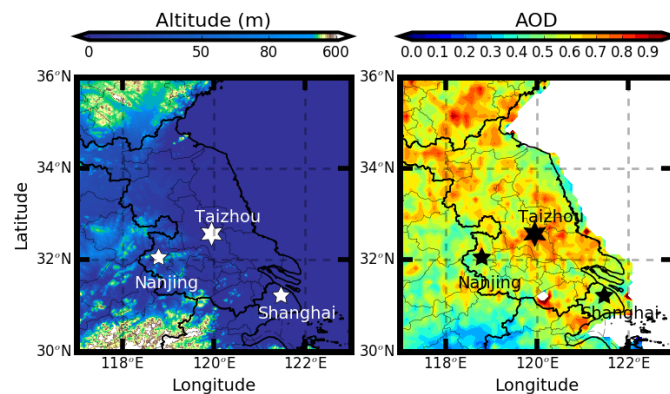


Figure 1: Measurement site of Taizhou (marked with stars). Filled colors represent (a) the topography of the Jianghuai Plain. (b) the average aerosol optical depth at 550nm during the year of 2017 from Moderate Resolution Imaging Spectroradiometer onboard satellite Aqua.

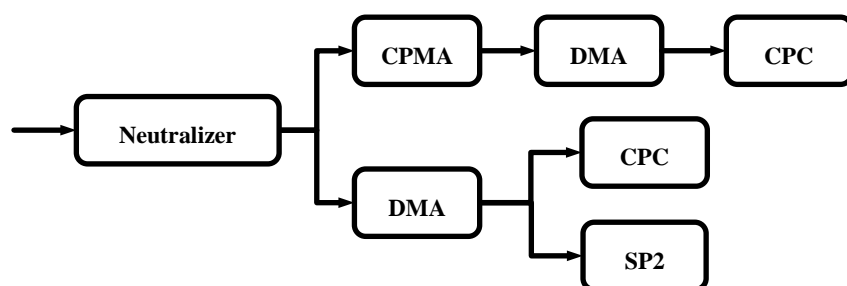
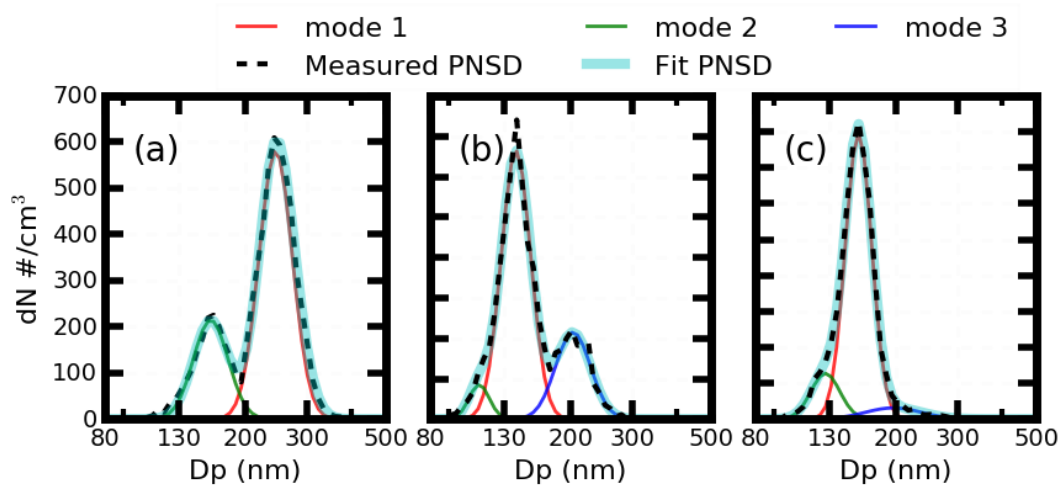


Figure 2. Schematic of the instrument setup.

518



519

520

521

522

523

Figure 3. The measured aerosol PNSD (black dotted line), fit aerosol number PNSD (blue solid line), and fit aerosol PNSD at three different mode in different colors that passed through the CPMA. Panel (a) (b) (c) corresponding to the aerosol mass concentrations of 12, 1 and 1.45 fg respectively.

524

525

526

527

528

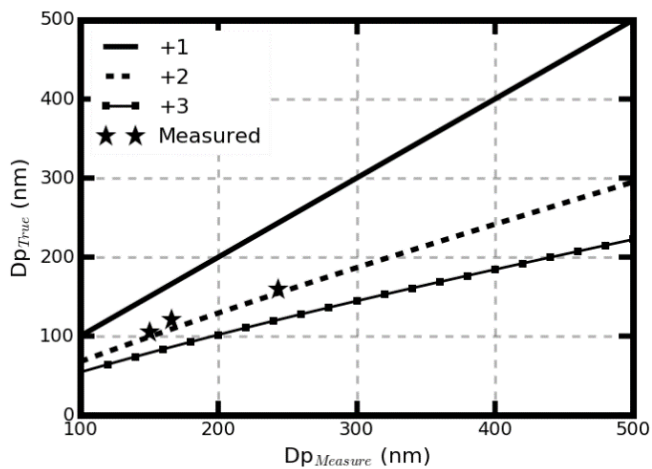
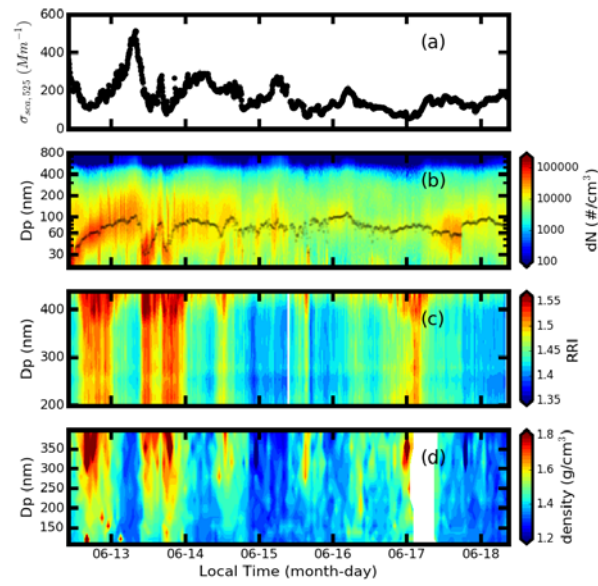


Figure 4. The relationship between the measured diameter by the DMA and the calculated aerosol diameter of different charges in the CPMA-SMPS system.

529

530



531

532

533

534

Figure 25. Time series of the measured (a) size-resolved RRI in filled color, σ_{sca} at 525nm in black dotted line and (b) the size-resolved ρ_{eff} .

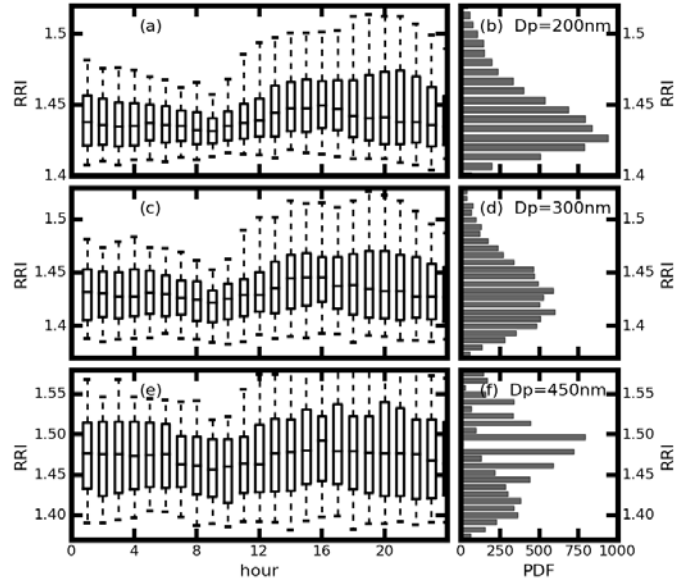


Figure 36. Daily variations of the RRI (a), (c) (e), and the probability distribution of the measured RRI (b), (d) (f) for the (a), (b) 200 nm, (c), (d) 300 nm, and (e), (f) 450nm aerosol respectively. The box and whisker plots represent the 5th, 25th, 75th and 95th percentiles.

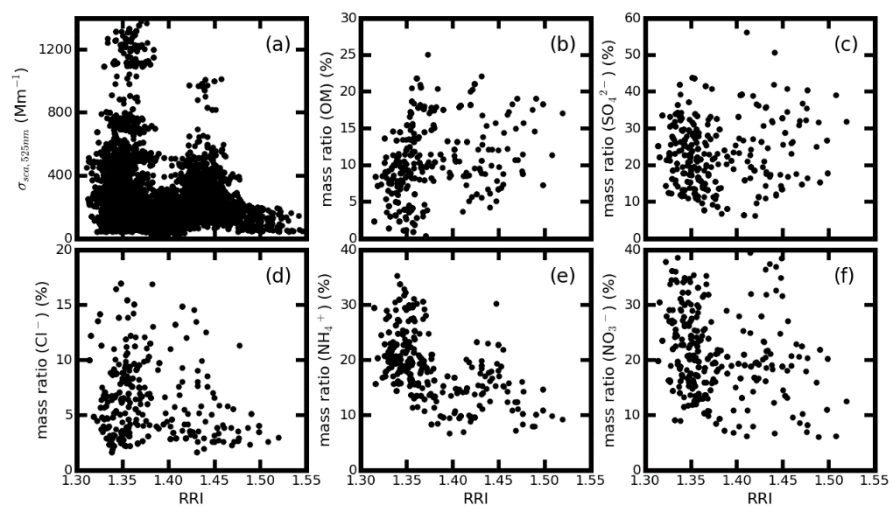


Figure 47. Comparison the measured RRI at 300nm with the measured (a) σ_{sca} at 525nm, mass fraction of (b) OM, (c) SO_4^{2-} , (d) Cl^- , (e) NH_4^+ and (f) NO_3^- .

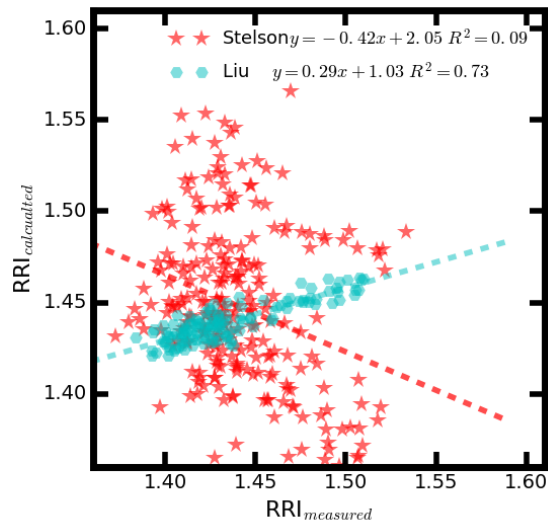
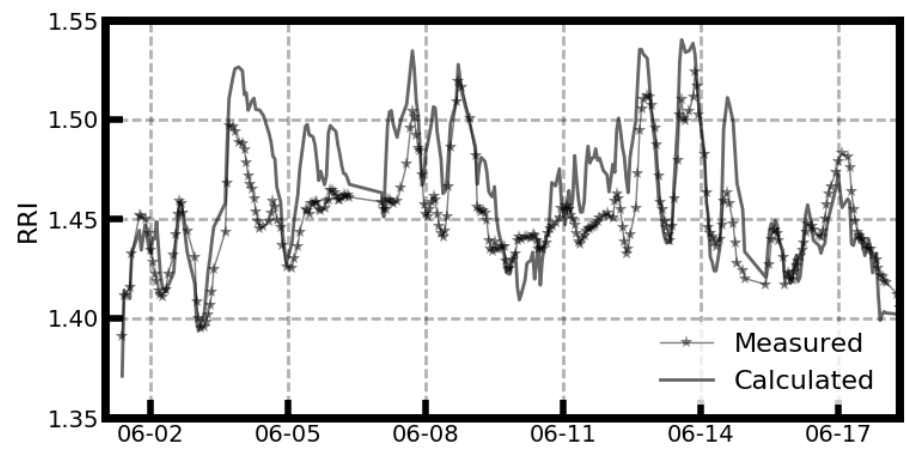


Figure 58. Comparison between the measured RRI and calculated RRI using the main aerosol chemical component ~~from~~ by applying the method of Stelson (1990) (in red star) and parameterization scheme proposed by Liu and Daum (2008) (in cyan hexagon).

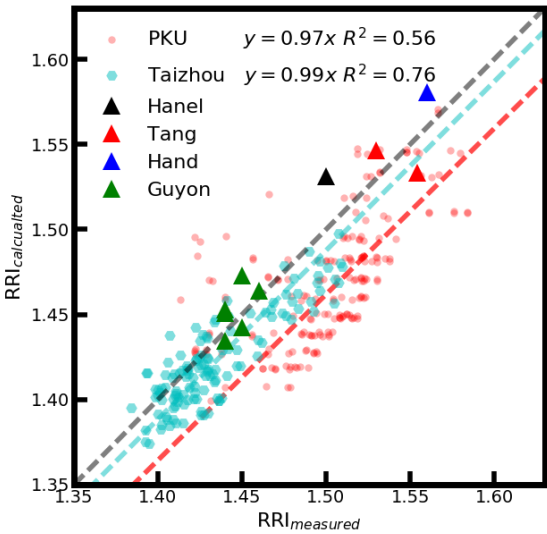
549



550

551 **Figure. 9.** Time series of the measured RRI at 250 nm and the calculated RRI using the aerosol bulk
552 aerosol optical properties.

553



555

556 **Figure 610.** Comparison between the measured and calculated RRI for different at PKU (in red
557 star circle) and Taizhou (in cyan hexagon) station. The triangle in black , red, blue and green
558 corresponding the data from Hänel (1968), Tang (1996), Hand and Kreidenweis (2002), and Guyon et
559 al. (2003) respectively. The black dashed line is the 1:1 line.

560

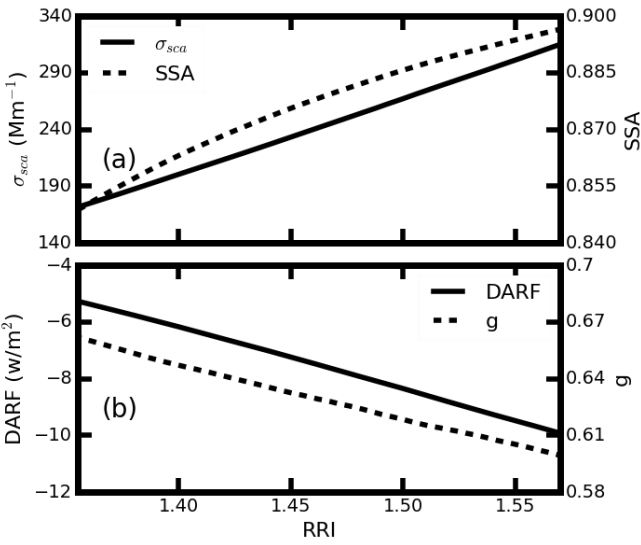


Figure 711. Variations of the estimated (a) σ_{sca} in solid line, SSA in dotted line, (b) g in dotted line, and DARF in solid line for different aerosol RRI.

Supplement for

A new parameterization scheme of the real part of the ambient aerosols refractive index

Gang Zhao¹, Tianyi Tan², Weilun Zhao¹, Song Guo², Ping Tian³, Chunsheng Zhao¹

1 Department of Atmospheric and Oceanic Sciences, School of Physics, Peking University, Beijing, China

2 State Key Joint Laboratory of Environmental Simulation and Pollution Control, College of Environmental Sciences and Engineering, Peking University, Beijing 100871, China

3 Beijing Key Laboratory of Cloud, Precipitation and Atmospheric Water Resources, Beijing 100089, China

1 The daily variation and probability distribution of the ρ_{eff}

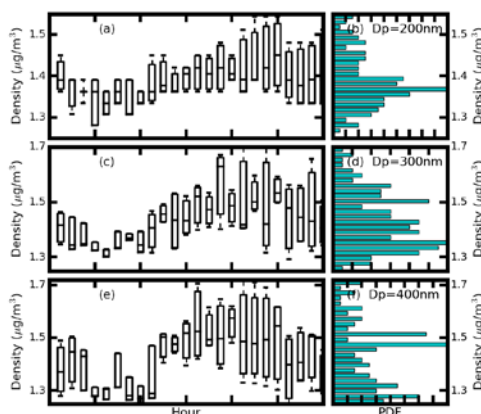


Figure. S1. Daily variations of the ρ_{eff} (a), (c) (e), and the probability distribution of the measured ρ_{eff} (b), (d) (f) for the (a), (b) 200 nm, (c), (d) 300 nm, and (e), (f) 400nm aerosol.

2. Comparison the measured RRI Aerosol Components

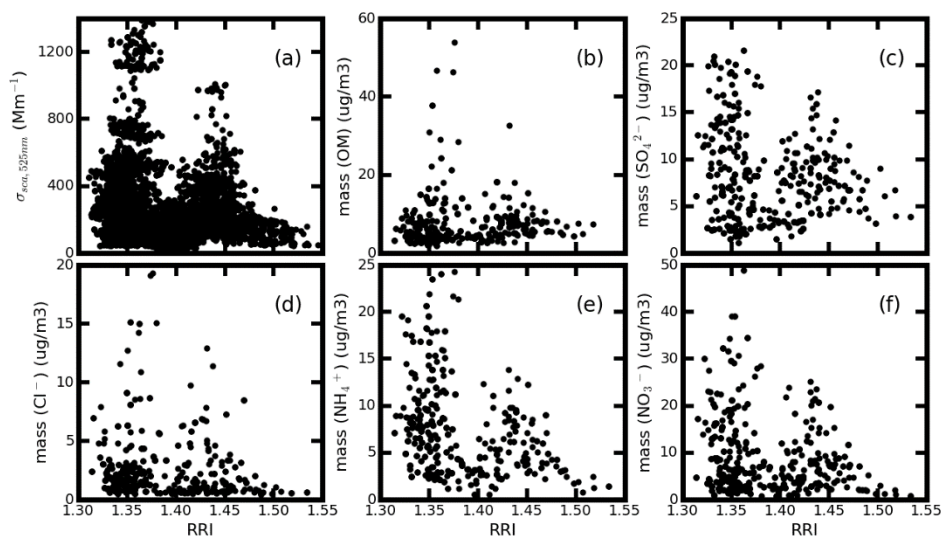


Figure S2. Comparison the measured RRI at 300nm with the measured (a) σ_{sca} at 525nm, mass concentrations of (b) OM, (c) SO_4^{2-} , (d) Cl^- , (e) NH_4^+ and (f) NO_3^- .